

Title	Ordered 2D colloidal photonic crystals on gold substrates by surfactant-assisted fast-rate Dip coating
Authors	Armstrong, Eileen;Khunshin, Worawut;Osiak, Michal J.;Blömker, Martin;Sotomayor Torres, Clivia M.;O'Dwyer, Colm
Publication date	2014-05
Original Citation	Eileen, A., Worawut, K., Michal, O., Martin, B., Sotomayor, T. C. M. and Colm, O. D. (2014) 'Ordered 2D Colloidal Photonic Crystals on Gold Substrates by Surfactant#Assisted Fast#Rate Dip Coating', Small, 10(10), pp. 1895-1901. doi: 10.1002/sml.201303616
Type of publication	Article (peer-reviewed)
Link to publisher's version	<a href="http://onlinelibrary.wiley.com/doi/10.1002/sml.201303616/full">http://onlinelibrary.wiley.com/doi/10.1002/sml.201303616/full</a> - 10.1002/sml.201303616
Rights	© 2014 WILEY#VCH Verlag GmbH & Co. KGaA, Weinheim. This is the peer reviewed version of the following article: Armstrong, E. , Khunshin, W. , Osiak, M. , Blömker, M. , Torres, C. M. and O'Dwyer, C. (2014), Ordered 2D Colloidal Photonic Crystals on Gold Substrates by Surfactant#Assisted Fast#Rate Dip Coating. Small, 10: 1895-1901, which has been published in final form at <a href="https://doi.org/10.1002/sml.201303616">https://doi.org/10.1002/sml.201303616</a> . This article may be used for non-commercial purposes in accordance with Wiley Terms and Conditions for Self-Archiving.
Download date	2025-06-01 07:27:22
Item downloaded from	<a href="https://hdl.handle.net/10468/6114">https://hdl.handle.net/10468/6114</a>

DOI: 10.1002/sml.((please add manuscript number))

**Article type: Communication**

**Ordered 2D Colloidal Photonic Crystals on Gold Substrates by Surfactant-assisted Fast-rate Dip Coating**

*Eileen Armstrong, Worawut Khunsin, Michael Osiak, Martin Blömker, Clivia M. Sotomayor Torres and Colm O'Dwyer\**

E. Armstrong,  
Department of Chemistry, University College Cork, Cork, Ireland

Dr. W. Khunsin  
Research Institute for Electronic Science, Hokkaido University, 001-0021 Sapporo, Japan.

M. Osiak  
Department of Chemistry, University College Cork, Cork, Ireland

M. Blömker  
Department of Chemical Engineering, Münster University of Applied Sciences,  
Stegerwaldstraße 39, 48565 Steinfurt, Germany

Prof. Dr. C. M. Sotomayor Torres  
Catalan Institute of Nanoscience and Nanotechnology ICN2, Campus UAB, Edifici ICN2,  
08193 Bellaterra, Spain  
and  
Catalan Institute for Research and Advanced Studies (ICREA), 08010 Barcelona, Spain

Dr. C. O'Dwyer  
Department of Chemistry, University College Cork, Cork, Ireland  
and  
Micro & Nanoelectronics Centre, Tyndall National Institute, Lee Maltings, Cork, Ireland  
and  
Materials & Surface Science Institute, University of Limerick, Limerick, Ireland

E-mail: [c.odwyer@ucc.ie](mailto:c.odwyer@ucc.ie)

We demonstrate how monolayer 2D colloidal photonic crystals or templates can be formed on gold substrates by dip-coating PMMA spheres at very fast (mm/min) withdrawal rates. Angle-resolved reflectance measurements confirm 2D light scattering characteristics from fast-rate dip-coated 2D PhCs with a high degree of surface ordering over large areas. The order was confirmed by scanning electron microscopy and is found to be facilitated when the micellular sodium dodecylsulfate surfactant is used above its critical micelle concentration. The technique can also provide ordered 3D colloidal crystals on gold substrates, where the degree of template ordering is controlled by variation of surfactant concentration, withdrawal rate and sphere concentration. The method allows high surface area and high throughput templating of metallic substrates in 2D or 3D for application in photonics, and as functional material templates for energy storage or sensors.

Keywords: colloids, template synthesis, monolayers, photonic crystals, self-assembly

Photonic crystals<sup>[1]</sup> (PhCs) most commonly self-assembled from mono-dispersed colloidal particles have been heavily investigated over the past decade due to their wide ranging applications in optics and optoelectronics, and more recently in electrochemical systems such as Li-ion batteries and electrochromics.<sup>[2, 3]</sup> Now highly adopted as an inexpensive and reliable means for the formation of both two-dimensional (2D) and three-dimensional (3D) ordered structures<sup>[4, 5]</sup>, they have proven attractive as stable templates for the formation of waveguides,<sup>[6]</sup> battery electrodes,<sup>[7, 8]</sup> optical switches,<sup>[9]</sup> and light-emitting diodes.<sup>[10]</sup> A variety of well-controlled methods<sup>[11]</sup> can be used to form these arrays, such as spin-coating,<sup>[12]</sup> drop-casting,<sup>[13]</sup> vertical deposition,<sup>[14]</sup> electrophoretic deposition,<sup>[15]</sup> dip-coating,<sup>[16, 17]</sup> Langmuir Blodgett,<sup>[18, 19]</sup> layer-by-layer assembly<sup>[20]</sup> or template directed growth.<sup>[21, 22]</sup> Advances in materials chemistry, that directly aid the assembly process, is critical for the function of templated 3D materials that are required for photonics, solar energy cells, and metamaterial constructs.

The requirements for near-perfection and zero defect tolerance is less stringent for some applications, particularly for templating materials for energy storage or sensing applications. Dip-coating is a widely used technique for the formation of colloidal 3D templates for functional porous materials, and is typically hindered from higher throughput by a slow rate of withdrawal. The control over evaporation rate and meniscus movement and characteristics are typically employed to ensure a well-ordered multilayer deposit of spheres.<sup>[17]</sup> In combination with controllable variables, such as temperature,<sup>[23]</sup> ionic strength control via charged colloids<sup>[24]</sup> or noise-induced stochastic resonance effect,<sup>[25]</sup> the coverage and long-range ordering can be improved, but all methods thus far rely on a very slow rate ( $\mu\text{m}/\text{min}$ ) of withdrawal to achieve thick and uniform opal deposits. This is especially important for template or PhC formation on gold or metallic substrates, and when using large diameter spheres. Langmuir-Blodgett techniques also limit conformal coverage to flat, non-

curved substrates. At faster rates (mm/min), i.e. far from equilibrium condition,<sup>[25]</sup> the spheres lack sufficient time to achieve an ordered crystallization and good adhesion to the substrate. With a non-functionalized silica or polymer sphere, typically used in assembling 3D opal templates, short- and long-range attractive Van der Waals forces<sup>[26]</sup> dominate over repulsive interactions from an electrical double layer. With no natural repulsion to assist ordering, the crystallization inevitably leads to a disordered and patched coverage of opal deposits on the substrate.

Forming opal templates on metallic surfaces, particularly those that can hold surface plasmon polaritons (SPPs) is proving important in advancing light-matter interactions in applications of hybrid plasmonic-photonic crystals and other complex heterostructures that benefit from plasmonic coupling within a photonic materials to a metallic substrate. Recent findings suggest that such metal-dielectric interfaces help reduce coupled light-leakage<sup>[27, 28]</sup> with potential application in enhanced solar cells, offer improvements in the quality factor for index-guided optical modes by a factor of  $\sim 10$ ,<sup>[29]</sup> and can enhance the light extraction efficiency of light emitters and the performance of photonic crystal based gas sensors<sup>[29, 30]</sup> Furthermore, this hybrid system finds beneficial applications as template for the fabrication of high-power, high rate battery electrodes,<sup>[8]</sup> and as substrates for surface-enhanced Raman scattering (SERS) measurements, since the template that is eventually infilled is directly connected to the current collector (substrate).<sup>[31]</sup> However, coating of gold substrates with colloidal crystals is not favourable under ambient conditions. This is because a clean gold substrate, free of any type of contaminants and naturally hydrophilic, quickly turns hydrophobic even with a monolayer of carbonaceous contamination.<sup>[32]</sup> As such, when in contact with air as in the most commonly used crystallization methods, the resulting structures are in most cases disordered crystals or amorphous structures.

Here, we show that surfactant functionalization of poly(methylmethacrylate) (PMMA) spheres of 700 nm in diameter allows a highly ordered 2D colloidal photonic crystal (PhC) to form on a gold surface, rather than glass substrates, by dip-coating at rates between 20 and 40 times faster than previously reported<sup>[24, 25]</sup>. In the absence of the surfactant, however, an amorphous, potentially uncorrelated, overlapping opal film is formed. In addition, we demonstrate how to achieve a multi-layer colloidal crystal template with a similar light scattering ability and coverage during coating at slower rate of withdrawal, using a lower concentration of spheres and surfactant. As will be shown, surfactant-assisted dip-coating provides a route to high quality ordered 2D or 3D colloidal crystals or templates directly on metallic surfaces at fast dip-coating rates.

The method is possible by using sodium dodecyl sulphate, which is an amphiphilic anion that dissociates in water to form charged monomers. At a sufficiently high concentration, greater than the critical micelle concentration (CMC), these monomers orientate their hydrophilic heads towards the polar solute, and their hydrophobic tails group together to form a hydrophobic core. These particles, known as micelles are known to enhance certain aspects of a solution such as the solubility of hydrophobic materials, and alter other aspects such as viscosity and polarity.<sup>[33]</sup> In our experiment, SDS was used at room temperature and at a concentration of 8 mg ml<sup>-1</sup>, above the theoretical CMC for SDS of 2.3 mg ml<sup>-1</sup> ( $8.0 \times 10^{-3}$  mol dm<sup>-3</sup>).<sup>[34]</sup> **Figure 1(a)** summarizes the dip coating of PMMA PhC monolayers and **Figure 1-(1-3)** illustrates the possible orientations of the SDS additive either in micellar and/or monomer form. At concentrations below CMC monomers of SDS are known to arrange along the water-air interface (**Figure 1-1**) but at the concentration level used in our experiment micellization of the SDS within solution takes precedence (**Figure 1-2**). At this point a transition from monomeric to micellized surfactant occurs at which point both micelles and monomers co-exist within the solution<sup>[35, 36]</sup> and any surfactant above CMC

will lead to the formation of micelles.<sup>[37]</sup> The full details and mechanisms for the SDS effects will be presented elsewhere but in brief, these micelles much like SDS does on an oil droplet,<sup>[38]</sup> can settle between or adsorb onto the surface of the PMMA spheres. A combination between the repulsive electrostatic forces induced beyond the Debye screening length in the electrical double layer of the sphere and depletion force kinetics can then cause an ordering of the spheres on removal from solution. The deposition was performed with a fast withdrawal rate of 1 mm/min, and SEM confirmed the resulting hexagonally packed monolayer of spheres. The sphere deposit exhibits large-scale surface coverage (over  $\sim 1 \text{ cm}^2$  of the substrate) of ordered domains (**Figure 1c**), a significant improvement over those achieved in the absence of SDS (**Figure 1b**) which were not only entirely disordered, but also displayed weak adhesion to the gold substrate. Micelle formation is expected and examinations of initial coagulation concentrations of SDS<sup>[39]</sup> show that the formation of a viscous mixture is possible and corresponds with the observation of improved order in deposits formed in the presence of micelles.

Without SDS, a monolayer is demonstrated to form, but does so as an amorphous photonic glass (**Figure 1b**). These deposits are also characterized by patchy coverage and regions of complete disorder. With SDS surfactant, the monolayer of 2D colloidal crystals can form from the fast rate (1 mm/min) of withdrawal with order and quality commensurate with the top surface ordering of multi-layered (3D) deposits reported previously for much slower rates ( $\mu\text{m}/\text{min}$ ).<sup>[25, 40]</sup> In the present case, the SDS lowers the surface tension causing a lengthening and thinning of the meniscus,<sup>[41]</sup> which we believe promotes the adhesion and crystallization of the spheres at the fast withdrawal rate. Local lattice distortions or vacancy defects in the 2D order (see **Figure 1c**) can be conveniently traced back to particle size distribution (see supporting information **Figure S3**), and shrinkage of the spheres during the

drying process, a common cause of cracks<sup>[42]</sup> usually observed in 3D PhCs by colloidal self-assembly.

In addition to lattice distortion, lattice misalignments in the monolayer 2D PhC are found to be caused mainly by the line dislocations stemming from anomalies in the close-packed 2D assembly. In particular, for this monolayer-type structure, these line dislocations merge to form the boundaries for the individual domains. The domain structure, however, remains well ordered and few rotational boundaries are found. The degree of order, which is shown by the effectively long-range polycrystalline order observed by hexagonal pattern in FFTs of the assembly (**Figure 1c**), is very high for a dip coating rate faster than typically used in dip-coating or Langmuir-Blodgett trough deposition. The 2D photonic glass monolayers (**Figure 1b**), while disordered on larger length scales, do contain some degree of small domains of frustrated hexagonal order with close-packed disorder surrounding these domains, evidenced by the spots in the FFT pattern (**Figure 1b**), that is largely characterized by diffuse rings symptomatic of a disordered (but not polycrystalline) arrangement.

The unique optical characteristics of opal-type photonic crystal templates<sup>[43, 44]</sup> allow for the investigation of their structural quality (assembly).<sup>[45, 46]</sup> Well-ordered 3D PhC structures show a specific photonic band-gap (PBG), the feature of which is observed at shorter wavelengths in the case of hexagonally ordered 2D opal PhCs, i.e. at  $\lambda \approx D$ , where  $D$  is the diameter of the spheres. These minima have been associated with excitation of 2D PhC optical eigenmodes that propagate along the plane of the monolayer opal.<sup>[28, 47]</sup> We note that we refer to the colloidal crystals with thickness of a few monolayer as principally 2D structures, due to the absence of appreciable 3D-related reflectance maxima obtained from the sample. In general, reflectance from a true 3D opal is related to its film thickness via Bragg attenuation length. In opals assembled from PMMA spheres of 700 nm in diameter, used in this experiment, the Bragg attenuation length is of the order of 6.5 to 7  $\mu\text{m}$  or



approximately 12 monolayers of spheres.<sup>[48]</sup> Furthermore, the presence of the reflectance maxima, i.e., photonic bandgap, quickly degrades in a disordered sample. It has been demonstrated with PMMA colloidal crystals that a defect vacancy of only 5% reduces the systems correlation length to a distance of  $3D$ , where  $D$  is the sphere diameter, resulting in the optical spectra being a simple incoherent scattering sum of individual Mie scatters without appreciable coherent PBG effect.<sup>[49]</sup> In our case of uncorrelated overlapping of 2D colloidal layers as seen in Fig. 1b, it is probably likely that the short correlation length due to large amount of defect vacancy present in the sample is the limiting factor to the absence of 3D optical feature.

The resonant scattering, thus formed by the coupling of the incident light with the guided mode of the 2D PhCs, provides an efficient and convenient means to characterize the 2D coverage and order within 2D opal films formed on a gold substrate at high drawing rate. The 2D PhCs, with thickness being far below the Bragg attenuation length, showed no three-dimensional order, as is evident by the lack of a photonic band gap within the expected range discussed above. Specifically, the corresponding 3D opal (111) plane stop band would appear at  $\sqrt{8/3} D \sqrt{g\bar{\epsilon}_s + (1-g)\bar{\epsilon}_f} \approx 1.6 \mu\text{m}$ , where  $\bar{\epsilon}_s$  and  $\bar{\epsilon}_f$  are the permittivity of PMMA and air between the spheres, and  $g$  is the maximum packing factor of  $g = \pi/3\sqrt{2}$  for the fcc lattice. The 2D monolayer opal, however, does scatter light in the visible range (at  $\lambda \approx D$ ) and can be conveniently detected with a Si CCD detector. **Figure 2a** shows the angle-resolved diffraction measurement obtained at angular increments of  $5^\circ$  for light incident at  $60^\circ$ . We note that the Fabry-Perot resonances are not observed from a single PhC layer as they are typically weaker and broader than diffraction contributions. Additionally, resonances from plasmonic interactions from the gold surface and their coupling to the 2D PhC, typically observed at wavelengths less than the sphere diameter are not observed, which is probably due to non-congruited gold surface and/or inefficient excitation of SPP at large incident

angle.<sup>[28]</sup> It is worth noting, however, that the lack of SPP excitation facilitates direct analysis of light scattering from the 2D monolayer colloidal crystals without being obscured by dispersion and broadening of scattering spectra due to the presence of a SPP.<sup>[50]</sup>

Confirmation of the structure of the 2D colloidal crystal formed is provided by analysis of the angle-resolved diffraction. The angular dispersion was fitted to the planar grating equation,  $\lambda = d[\sin(\alpha) + \sin(\beta + x)]$ , where  $\alpha$  is the angle of incidence,  $\beta$  is the angle of diffraction,  $d$  is the effective grating groove, which in this case corresponds to  $\frac{\sqrt{3}}{2}D$ , the half period of the trigonal lattice for the wave vector of incident light propagating along the  $\Gamma K$  direction in the Brillouin zone of a 2D hexagonal lattice. This is schematically represented in Figure 2(b), where  $D$  is the sphere diameter, and  $x$  is the deviation half-angle between incident and diffracted beams defined according to  $\alpha(\lambda) = \beta(\lambda) + 2x$ . **Figure 2b** shows the theoretical dispersion (blue line) calculated using the equation above with the nominal diameter of 700 nm for the spheres, as determined by SEM and dynamic light scattering, as an input parameter. The fitting procedure gives  $x \sim 10.57$ , the result of which is plotted against the experimental dispersions (black circles) taken from the experimental spectra shown in **Figure 2a**. The red dashed line indicates the ‘best fit’ theoretical dispersion i.e. when the diameter of the spheres is not fixed at 700 nm. This calculation suggests a slight increase in the diameter of the spheres which could be related to the SDS addition and its presence around the spheres (see supporting information **Figure S4**).

**Figure 2(c)** shows the light scattering behaviour for a fast-rate dip-coated 2D PhC monolayer formed with SDS surfactant at a diffraction angle of  $0^\circ$ , i.e. normal to the substrate, for light incident at  $60^\circ$ , and is compared to the same response for the photonic glass deposit in the absence of SDS (black line). In this latter case, no 2D scattering was observed. The scattering spectra of the PhC monolayer (red line) formed in the presence of SDS exhibited well-defined scattering characteristic of a 2D colloidal crystal at a reduced

wavelength of  $D/\lambda = 1.13$ , close to the scattering resonance condition for the monolayer opal. The disordered monolayer breaks the Bragg scattering condition, causing additional background scattering components, which can be observed as a broadband, low-intensity peak shown in **Figure 2c**. The profile does follow somewhat the diffraction of the ordered 2D opal and is likely due to the small degree of ordering within several domains (see **Figure 1b**).

Controlled experiments were performed at a slow rate of withdrawal, with and without SDS. In absence of SDS, we did not observe any formation of colloidal crystals on the gold substrate, which is likely due to the difficulty of assembling on the gold surface for PMMA spheres as mentioned above as opposed to at the fast rate of withdrawal, which is probably due to spontaneous fixing of the spheres onto the substrate by the fast advancing meniscus.<sup>[51]</sup> Dip coating experiments with the addition of SDS, identical to that reported in **Figure 2**, but at a slow rate of  $\sim 1$  mm/hr comparable to that reported by Khunsin *et al.*<sup>[25]</sup> produced a sample of patched coverage and poor order, the thickness of which varies across several areas of the sample to a greater extent than the fast rate sample (compare **Figure 1c** and **Figure S1**). Slower withdrawal from the same sphere-containing solution did not induce an ordered opal monolayer. However, a reduction in sphere concentration by half with a parallel reduction in SDS concentration to  $4 \text{ mg ml}^{-1}$ , i.e. maintaining the same ratio of spheres to SDS as the fast rate sample, but still above critical micelle concentration, resulted in a better quality PhC structure, as shown in **Figure 3(b)**. The morphology is comparable to the monolayer formed at  $1 \text{ mm/min}$  with twice the concentration of spheres and SDS (**Figure 1c**). Scattering data acquired with light incident at  $45^\circ$  and a similar angular shift in peak position was measured indicating the presence of 2D order within the template, as shown in **Figure 3(a)**. A comparison of the scattering from the fast and slow rate 2D PhCs for light incident at the same angle  $45^\circ$  is shown in **Figure 3(c)**, where the scattering peak for the fast rate sample is located at a wavelength of  $D/\lambda = 1.13$ , whereas that of a deposit formed with

half the concentration of spheres and SDS is located at  $D/\lambda = 1.2$ . We note that the scattering peak for the fast rate sample is ~15% broader than the 2D PhC formed at the slow rate, which indicates a lesser degree of order in the fast rate sample. This might be due to larger crystal lattice distortion from dislocations and/or concentration gradients, i.e. non-uniform distribution of the spheres, and contributions from wider spaces between spheres in the case of fast rate sample with double the concentration of spheres and SDS.<sup>[52]</sup> It is noted, however, that the PhC achieved for the slow rate with reduced concentration is not a single monolayer of spheres as seen for the faster rate sample; the increase in thickness while not sufficient to produce a 3-dimensional structure provides an environment that is more conducive to crystallization of the spheres,<sup>[25]</sup> leading to extended long-range order for this slow rate sample and explains the lower relative bandwidth ( $\Delta\lambda/\lambda$ ) of 0.052 compared with that of 0.067 for the fast rate dip-coated PhC (**Figure 3c**).

The dispersion of the scattering maximum obtained from both samples show excellent agreement with calculated 2D diffraction from grating theory, as seen from the line fits in **Figure 4a and 4b**. However, we note two important differences between the two samples in the absolute position (wavelength) of the scattering maxima and the width of the resonances. The larger diffraction wavelengths, in the case of the slow rate sample, is due to two contributing factors: (1) larger effective diameter due to higher SDS concentration which leads to a thick coating of micellar SDS around the spheres (see **Figure S4**), and (2) the increase in effective refractive index of the inter-sphere medium (which is nominally air) due to the coating of SDS. **Figure 4c** plots the dispersions of the ratio of the Full-Width Half-Maximum (FWHM) to the resonant wavelengths of the diffraction peaks as a function of diffraction angle for both the fast-rate sample, and the slow-rate sample. The lower overall ratio, i.e. narrower diffraction peaks, indicates less scattering from imperfection in the crystal lattice and thus implies the improved order of the slow rate sample compared to the fast rate

sample. Along the same line of the above arguments, we believe that the slow rate sample possesses better ordering due to a thinner and more uniform coating of SDS on the surface of the spheres than the fast rate sample. Further work into the optimum SDS concentration for the deposition of PMMA spheres on gold substrates is undergoing and will be reported elsewhere.

To conclude, the fast-rate dip coating has been successfully demonstrated in the formation of an ordered 2D monolayer colloidal crystal of polymer (PMMA) spheres on a gold substrate when a surfactant such as SDS is mixed into the sphere solution *prior* to dipping. For the same concentration of spheres and SDS as is used when dip-coating at the faster rate, assembly of polymer (PMMA) spheres as a colloidal 2D PhC monolayer on gold coated silicon is less effective at a slow rate of withdrawal and typically results in a disordered monolayer. However, a reduction in the concentration of both spheres and SDS by 50% improves the deposition at a slow rate as evidenced by angle-resolved light scattering measurements, surpassing that obtained with the fast rate deposition. The findings demonstrate that higher quality 2D colloidal crystals of polymer spheres can be formed on gold substrates with the addition of SDS surfactant, when dip-coating at fast or slow rates, provided concentrations are controlled (in this case lowered) at slower rates, thus overcoming the difficulty associated with the hydrophobicity of the gold substrate at ambient conditions. Our result may pave the way for the development of hybrid 2D and/or 3D opal photonic-plasmonic structures for applications in high-sensitivity bio- and chemical sensors, and as high-throughput templates on conductive surfaces for functional porous electrodes for energy storage/batteries, and as substrates for SERS experiments. Furthermore, the method can particularly be adapted to deposition methods of ordered monolayers that are typically limited to slower withdrawal or deposition rates.<sup>[53]</sup> The ability to control the assembled of 2- and 3D colloidal crystals may also aid the controlled evaporative self-assembly of binary or tertiary

colloidal structures and photonic crystals composed of blends of templates and active emitters or absorbers, and do so on metallic surfaces that hold surface plasmon excitations for a wide variety of optical applications. Advances in template fabrication directly on metallic, conductive substrates at higher fabrication rates, without a reduction in ordering, are also particularly useful for sensing and energy storage architectures such as fast charging rate high power Li-ion microbatteries and related structures that rely on controlled porosity in the active materials.

### Experimental Details

A silicon wafer was cleaned in  $\text{Ar}^+$  plasma and coated with 10 nm titanium adhesion layer and 100-150 nm gold by ion beam sputtering using an ATC Orion-5-UHV sputtering system. A piece approximately  $1\text{ cm} \times 1\text{ cm}$  was then cleaned in nitric acid for  $\sim 2$  hr, and rinsed with deionized water. Mono-dispersed PMMA spheres with diameter  $D \sim 700$  nm, synthesized with altered concentrations according to the method outlined by Schroden,<sup>[54]</sup> were centrifuged and dried at  $50^\circ\text{C}$  and redistributed in distilled water with a concentration of 5 wt%. The surfactant used was sodium dodecyl sulfate (SDS), used as received from Sigma-Aldrich, at a concentration of  $8\text{ mg ml}^{-1}$  ( $27.7 \times 10^{-3}\text{ mol dm}^{-3}$ ), far greater than the theoretical critical micelle concentration (CMC) of  $2.3\text{ mg ml}^{-1}$  ( $8.0 \times 10^{-3}\text{ mol dm}^{-3}$ ).<sup>[34, 55]</sup> The clean substrate was then settled vertically into the sphere solution and removed, as schematically shown in Figure 1, at a high rate of 1 mm/min using a MTI Corporation PTL-MM01 Dip Coater apparatus.

Characterization of the PhC ordering was probed by angle-resolved spectroscopy in a monochromator-mount configuration on a rotating stage with fixed incident angles of  $60^\circ$  and  $45^\circ$ . The sample was illuminated with white light from a Halogen bulb collimated to a beam diameter of  $\sim 1$  mm. Spectra of the planar diffracted light were collected with at an interval of

5° and an angular resolution of 2° using a CCS200 Compact CCD spectrometer in the wavelength range 200 – 1000 nm. Scanning electron microscopy (SEM), performed on a Hitachi S-4800 field emission SEM, was used to visualize the in-plane (top layer) ordering of the samples.

### **Supporting Information**

Supporting Information is available online from the Wiley Online Library or from the author.

### **Acknowledgements**

EA and MO acknowledge the support of the Irish Research Council under awards RS/2010/2920 and RS/2010/2170. WK and CMST acknowledge support from the Spanish National I+D Plan projects TAPHOR (MAT-2012-31392) and CONSOLIDER nanoTHERM (CSD2010-00044). COD acknowledges support from Science Foundation Ireland under award no. 07/SK/B1232a-STTF11, the UCC Strategic Research Fund, and from the Irish Research Council New Foundations Award.

Received: ((will be filled in by the editorial staff))  
Revised: ((will be filled in by the editorial staff))  
Published online: ((will be filled in by the editorial staff))

## References

- [1.] A. Stein; R. C. Schroden, *Curr. Opin. Solid State Mater. Sci.* **2001**, 5 (6), 553-564.
- [2.] J. F. Galisteo-López; M. Ibisate; R. Sapienza; L. S. Froufe-Pérez; Á. Blanco; C. López, *Adv. Mater.* **2011**, 23 (1), 30-69.
- [3.] A. Stein; B. E. Wilson; S. G. Rudisill, *Chem. Soc. Rev.* **2013**, 42 (7), 2763-2803.
- [4.] C. López, *Adv. Mater.* **2003**, 15 (20), 1679-1704.
- [5.] P. V. Braun, *Chem. Mater.* **2013**, 10.1021/cm4023437.
- [6.] L. Lu; J. D. Joannopoulos; M. Soljačić, *Phys. Rev. Lett.* **2012**, 108 (24), 243901.
- [7.] J. S. Sakamoto; B. Dunn, *J. Mater. Chem.* **2002**, 12 (10), 2859-2861.
- [8.] H. Zhang; X. Yu; P. V. Braun, *Nat. Nanotechnol.* **2011**, 6, 277-281.
- [9.] Y. Liu; F. Qin; Z.-Y. Wei; Q.-B. Meng; D.-Z. Zhang; Z.-Y. Li, *Appl. Phys. Lett.* **2009**, 95 (13), 131116.
- [10.] E. Yablonovitch, *J. Opt. Soc. Am. B* **1993**, 10 (2), 283-295.
- [11.] G. von Freymann; V. Kitaev; B. V. Lotsch; G. A. Ozin, *Chem. Soc. Rev.* **2013**, 42 (7), 2528-2554.
- [12.] M. Pichumani; P. Bagheri; K. M. Poduska; W. Gonzalez-Vinas; A. Yethiraj, *Soft Matter* **2013**, 9 (12), 3220-3229.
- [13.] O. D. Velev; K. Furusawa; K. Nagayama, *Langmuir* **1996**, 12 (10), 2374-2384.
- [14.] P. Jiang; J. F. Bertone; K. S. Hwang; V. L. Colvin, *Chem. Mater.* **1999**, 11 (8), 2132-2140.
- [15.] A. L. Rogach; N. A. Kotov; D. S. Koktysh; J. W. Ostrander; G. A. Ragoisha, *Chem. Mater.* **2000**, 12 (9), 2721-2726.
- [16.] C. Deleuze; B. Sarrat; F. Ehrenfeld; S. Perquis; C. Derail; L. Billon, *Phys. Chem. Chem. Phys.* **2011**, 13 (22), 10681-10689.
- [17.] A. S. Dimitrov; K. Nagayama, *Langmuir* **1996**, 12 (5), 1303-1311.
- [18.] B. van Duffel; R. H. A. Ras; F. C. De Schryver; R. A. Schoonheydt, *J. Mater. Chem.* **2001**, 11 (12), 3333-3336.
- [19.] M. Bardosova; P. Hodge; L. Pach; M. E. Pemble; V. Smatko; R. H. Tredgold; D. Whitehead, *Thin Solid Films* **2003**, 437 (1-2), 276-279.
- [20.] J. R. Oh; J. H. Moon; S. Yoon; C. R. Park; Y. R. Do, *J. Mater. Chem.* **2011**, 21 (37), 14167-14172.
- [21.] A. Van Blaaderen; R. Ruel; P. Wiltzius, *Nature* **1997**, 385, 321-324.
- [22.] C. Jin; M. A. McLachlan; D. W. McComb; R. M. De La Rue; N. P. Johnson, *Nano Lett.* **2005**, 5 (12), 2646-2650.
- [23.] Y. Fu; Z. Jin; Z. Liu; Y. Liu; W. Li, *Mater. Lett.* **2008**, 62 (27), 4286-4289.
- [24.] K. W. Tan; Y. K. Koh; Y.-M. Chiang; C. C. Wong, *Langmuir* **2010**, 26 (10), 7093-7100.
- [25.] W. Khunsin; A. Amann; G. Kocher-Oberlehner; S. G. Romanov; S. Pullteap; H. C. Seat; E. P. O'Reilly; R. Zentel; C. M. S. Torres, *Adv. Funct. Mater.* **2012**, 22 (9), 1812-1821.
- [26.] J. Chen; A. Anandarajah, *J. Colloid Interface Sci.* **1996**, 180 (2), 519-523.
- [27.] S. G. Romanov; A. V. Korovin; A. Regensburger; U. Peschel, *Adv. Mater.* **2011**, 23 (22-23), 2515-2533.
- [28.] S. G. Romanov; N. Vogel; K. Bley; K. Landfester; C. K. Weiss; S. Orlov; A. V. Korovin; G. P. Chuiko; A. Regensburger; A. S. Romanova; A. Kriesch; U. Peschel, *Phys. Rev. B* **2012**, 86 (19).
- [29.] X. D. Yu; L. Shi; D. Z. Han; J. Zi; P. V. Braun, *Adv. Funct. Mater.* **2010**, 20 (12), 1910-1916.
- [30.] M. López-García; J. F. Galisteo-López; A. Blanco; J. Sánchez-Marcos; C. López; A. García-Martín, *Small* **2010**, 6 (16), 1757-1761.



- [31.] S. Kubo; Z.-Z. Gu; D. A. Tryk; Y. Ohko; O. Sato; A. Fujishima, *Langmuir* **2002**, *18* (13), 5043-5046.
- [32.] T. Smith, *J. Colloid Interface Sci.* **1980**, *75* (1), 51-55.
- [33.] C. C. Ruiz, *Colloids Surf., A* **1999**, *147* (3), 349-357.
- [34.] E. A. G. Aniansson; S. N. Wall; M. Almgren; H. Hoffmann; I. Kielmann; W. Ulbricht; R. Zana; J. Lang; C. Tondre, *J. Phys. Chem.* **1976**, *80* (9), 905-922.
- [35.] N. J. Turro; A. Yekta, *J. Am. Chem. Soc.* **1978**, *100* (18), 5951-5952.
- [36.] S. Freire; J. Bordello; D. Granadero; W. Al-Soufi; M. Novo, *Photochem. Photobiol. Sci.* **2010**, *9* (5), 687-696.
- [37.] W. Al-Soufi; L. Piñeiro; M. Novo, *J. Colloid Interface Sci.* **2012**, *370* (1), 102-110.
- [38.] M. A. James-Smith; K. Alford; D. O. Shah, *J. Colloid Interface Sci.* **2007**, *310* (2), 590-598.
- [39.] I. M. Umlong; K. Ismail, *Colloids Surf., A* **2007**, *299* (1-3), 8-14.
- [40.] W. Khunsin; G. Kocher; S. G. Romanov; C. M. S. Torres, *Adv. Funct. Mater.* **2008**, *18* (17), 2471-2479.
- [41.] H. H. Wickman; J. N. Korley, *Nature* **1998**, *393*, 445-447.
- [42.] M. A. McLachlan; N. P. Johnson; R. M. De La Rue; D. W. McComb, *J. Mater. Chem.* **2005**, *15* (3), 369-371.
- [43.] S. John, *Phys. Rev. Lett.* **1987**, *58* (23), 2486-2489.
- [44.] E. Yablonovitch, *Phys. Rev. Lett.* **1987**, *58* (20), 2059-2062.
- [45.] G. Lozano; L. A. Dorado; D. Schinca; R. A. Depine; H. Míguez, *Langmuir* **2009**, *25* (22), 12860-12864.
- [46.] S. G. Romanov; M. Bardosova; M. Pemble; C. M. S. Torres, *Appl. Phys. Lett.* **2006**, *89* (4), 043105-3.
- [47.] S. Peng; G. M. Morris, *J. Opt. Soc. Am. A* **1996**, *13* (5), 993-1005.
- [48.] W. Khunsin; S. G. Romanov; C. M. S. Torres; J. Ye; R. Zentel, *J. Appl. Phys.* **2008**, *104* (1), 013527.
- [49.] P. D. Garcia; R. Sapienza; C. Toninelli; C. Lopez; D. S. Wiersma, *Phys. Rev. A* **2011**, *84* (2).
- [50.] B. Ding; M. Bardosova; M. E. Pemble; A. V. Korovin; U. Peschel; S. G. Romanov, *Adv. Funct. Mater.* **2011**, *21* (21), 4182-4192.
- [51.] P. A. Kralchevsky; N. D. Denkov, *Curr. Opin. Colloid Interface Sci.* **2001**, *6* (4), 383-401.
- [52.] R. G. Shimmin; A. J. DiMauro; P. V. Braun, *Langmuir* **2006**, *22* (15), 6507-6513.
- [53.] Z. Dai; Y. Li; G. Duan; L. Jia; W. Cai, *ACS Nano* **2012**, *6* (8), 6706-6716.
- [54.] R. C. Schroden; N. Balakrishnan, *Inverse Opal Photonic Crystals: A Laboratory Guide*. University of Minnesota Materials Research Science and Engineering Center: University of Minnesota, Amundson Hall 491, 421 Washington Ave. SE, Minneapolis, MN 55455, **2001**.
- [55.] P. Lianos; R. Zana, *J. Colloid Interface Sci.* **1981**, *84* (1), 100-107.

### Figure captions

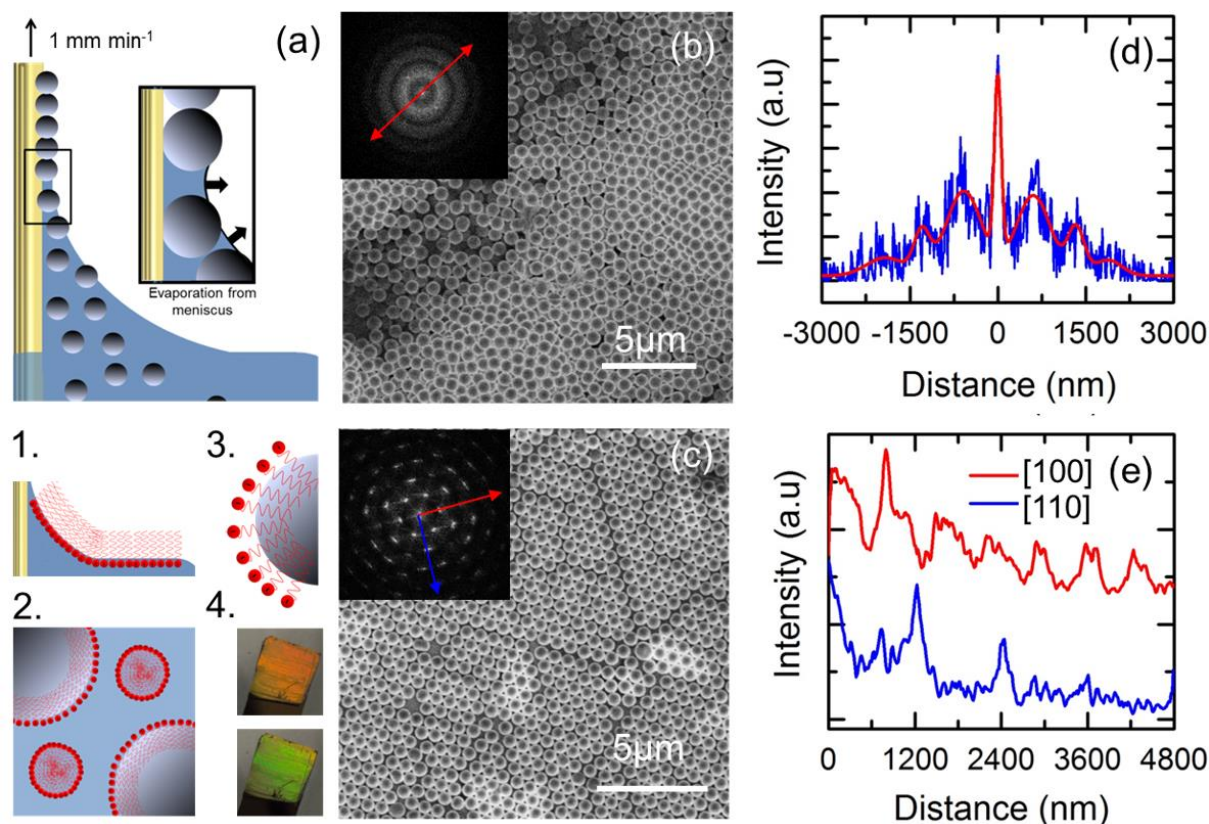


**Figure 1.** (a) Diagram depicting the deposition mechanism of opal spheres by dip coating at a withdrawal rate of 1 mm/min. (1-4) Schematic representation of micellar SDS and functionalized PMMA and optical images of the angle-dependent scattering seen from PhC deposits formed using SDS. (b) SEM image and corresponding FFTs showing a 2D photonic glass monolayer (without SDS) and (c) a 2D monolayer photonic crystal (with SDS) and (d) and (e) are the FFT intensity profiles from (b) and (c) respectively. Profiles in (e) were acquired along the [100] and [110] directions, corresponding to the  $\Gamma X$  and  $\Gamma L$  directions in the Brilluoin zone of a 2D hexagonal lattice.

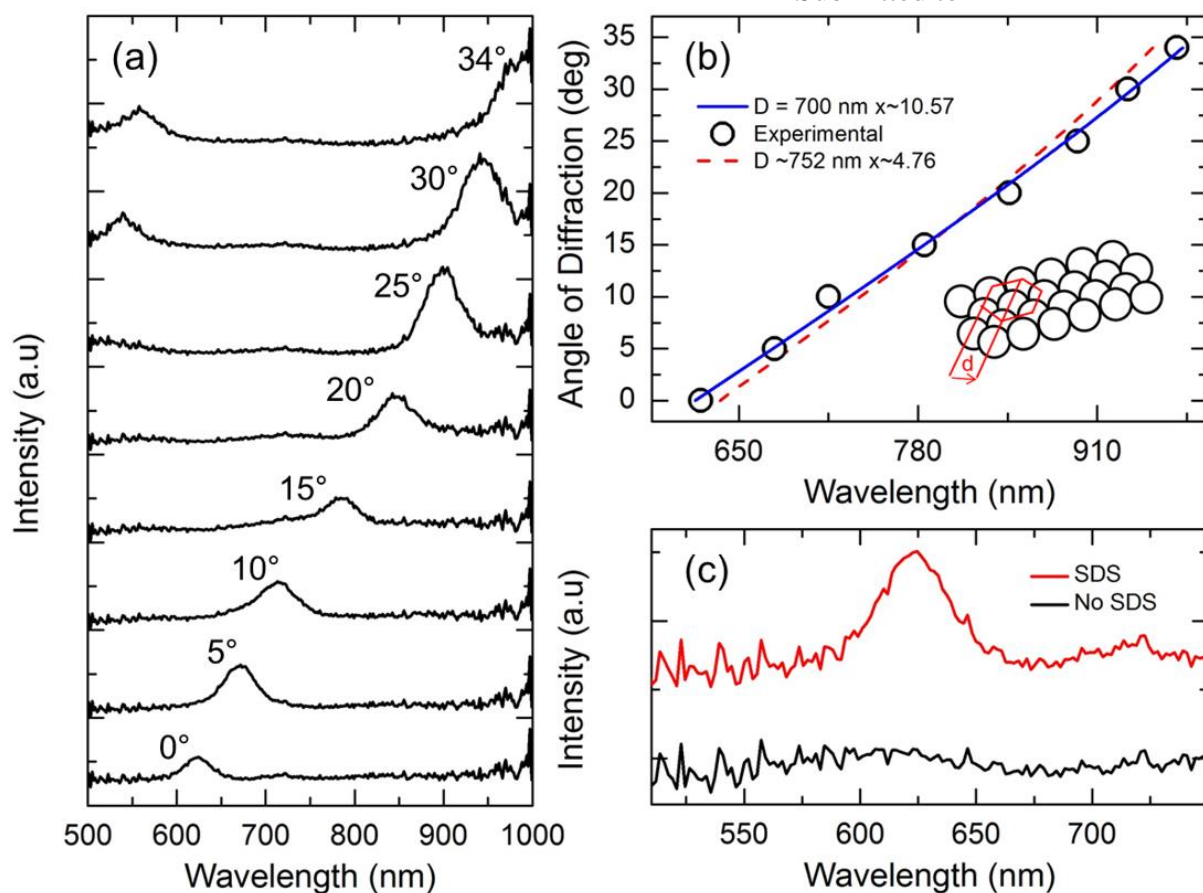


**Figure 2.** Dispersion characterisation (a) Angle-resolved scattering for 5 wt% PMMA spheres with  $8 \text{ mg ml}^{-1}$  SDS at an incident angle of  $60^\circ$ . (b) The dispersion of the peak position compared with the theoretical dispersion and the schematic representation of the grating groove  $d$ , and (c) Light scattering normal to the surface (i.e. angle of diffraction =  $0^\circ$ ) for light incident at  $60^\circ$ .

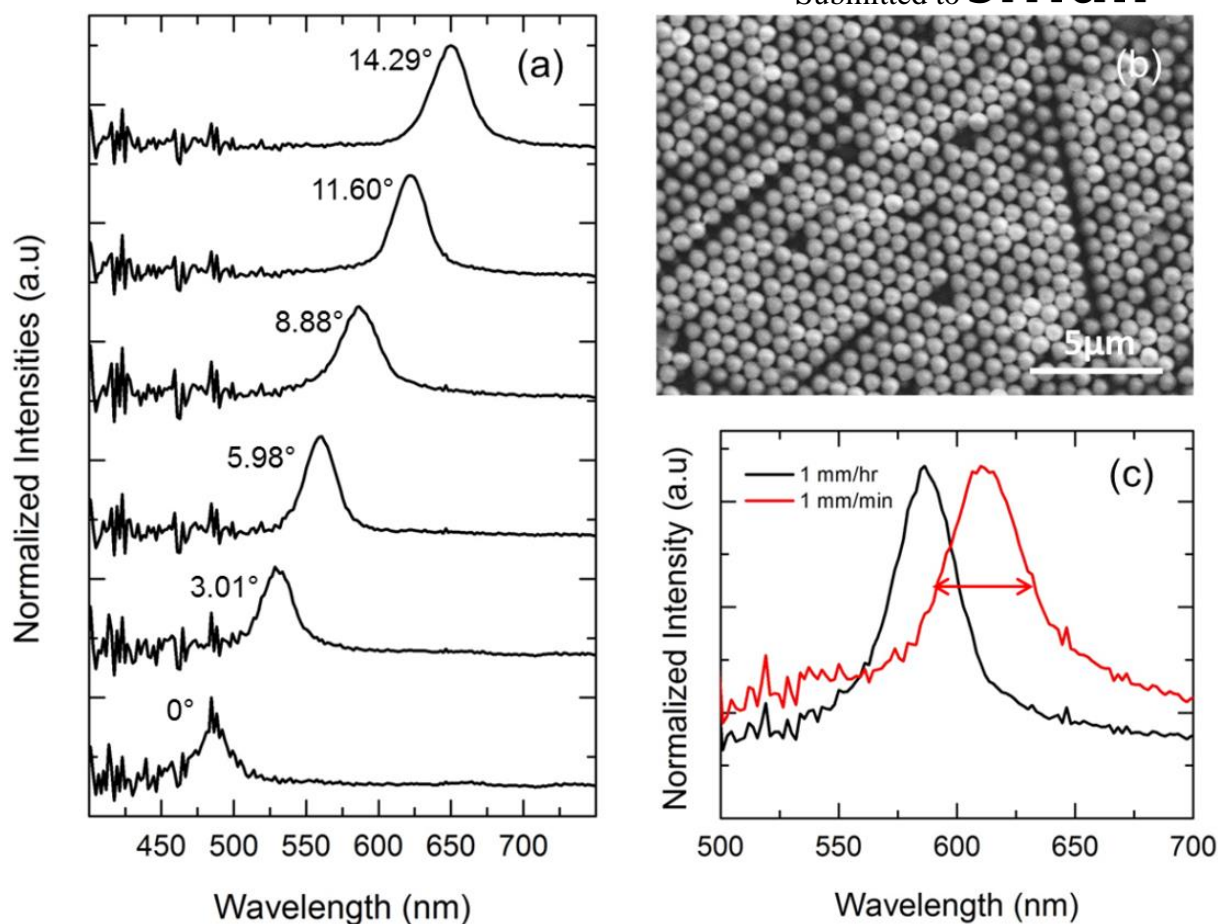


**Figure 3.** (a) Angle resolved scattering from the 2D PhC formed from 2.5 wt% PMMA spheres with  $4 \text{ mg ml}^{-1}$  SDS dip coated at a slow rate ( $\sim 1 \text{ mm/hr}$ ). Light was incident at  $45^\circ$ . (b) SEM image of the top surface of the 2D PhC. (c) Scattering at an angle of  $8.88^\circ$  for light incident at  $45^\circ$  for samples formed at fast rate with 5 wt% spheres and  $8 \text{ mg ml}^{-1}$  SDS (red), and for a sample formed at the slow rate where the concentrations of spheres and SDS are halved (black).

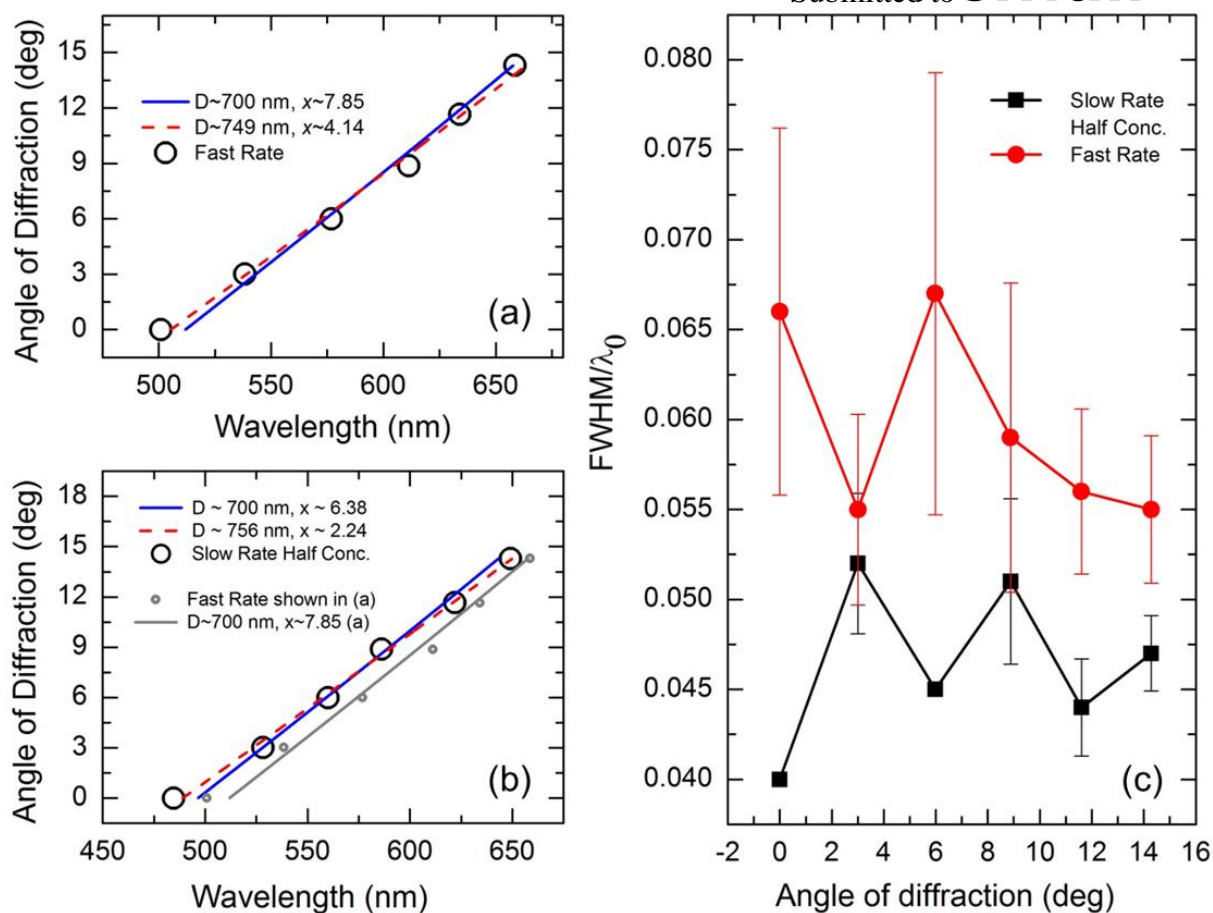


**Figure 4.** (a) The dispersion relation for a sample made using 5 wt% PMMA spheres and 8 mg ml<sup>-1</sup> SDS withdrawn at a fast rate (~1 mm/min) when light is incident at 45°. (b) The dispersion relation for the scattering spectra shown in Figure 3a (2.5 wt% PMMA spheres and 4 mg ml<sup>-1</sup> SDS), the grey line shows the plot in (a) again for comparison, the variation we purpose is due to the increased SDS concentration and (c) shows a plot of the ratio of the resonant wavelength to the FWHM for both samples.